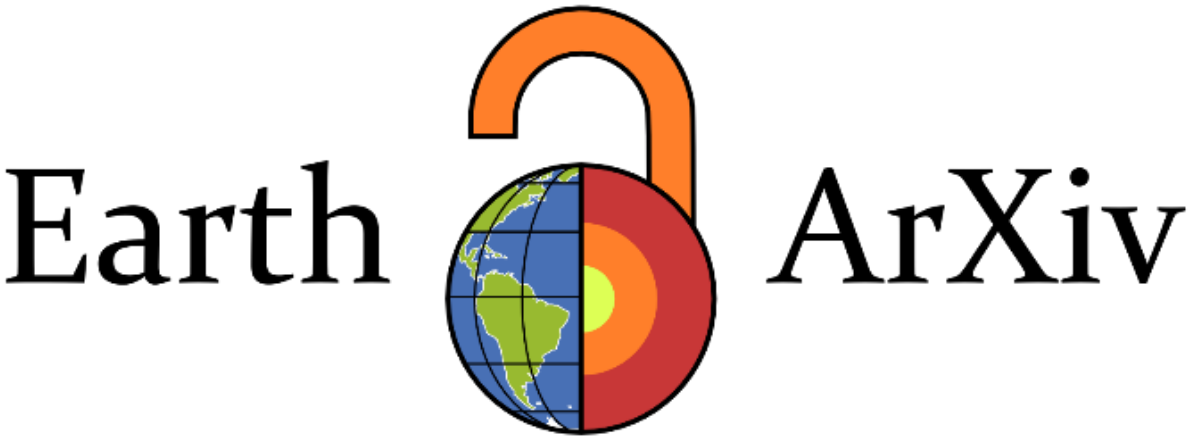

Global warming strengthens atmospheric ducting

Xiaofeng Zhao[1†*], Chunshan Wei[2†], Dongxiao Wang[3], Xiaoqian Zhu[2], Pinglv Yang[1] and Yudi Liu[1]

[1*]Meteorology and Oceanography, NUDT, Changsha, 410073, China.

[2]Command and Control Engineering, AEU, Nanjing, 210017, China.

[3]School of Marine Sciences, Sun Yat-Sen University, Zhuhai, 519000, China.

*Corresponding author(s). E-mail(s): zhaoxiaofeng@nudt.edu.cn

†These authors contributed equally to this work.

Abstract

Atmospheric ducts (ADs) provide efficient electromagnetic wave channels for beyond line-of-sight (BLOS) propagation and can serve as a sensitive diagnostic factor for the change of lower atmosphere. Based on the ERA5 model-level reanalysis data (1979–2024), a global-scale assessment of the response of AD evolution to global warming has been revealed for the first time. The occurrence probability, strength, and top height of AD all exhibit an increasing trend over mid- to low-latitude oceans. Analysis of underlying physical mechanisms indicates that this long-term trend is highly coupled with the continuous increase in atmospheric static stability within the lower marine atmosphere in the context of global warming. While interannual variability—typified by the El Niño–Southern Oscillation—modulates the amplitude of these anomalies, the long-term trajectory is overwhelmingly dictated by the secular trend. Ultimately, continuous warming is shifting the marine atmospheric background state toward a regime favoring more frequent and intense ducting, with profound implications for maritime BLOS communication and radar detection.

Keywords: Global Warming, Atmospheric Duct, ENSO

1 Introduction

Atmospheric ducts (ADs) are anomalous stratification layers defined by a negative vertical gradient of modified refractivity. Acting as natural waveguides, these layers trap electromagnetic energy to minimize propagation loss; while this enables beyond-line-of-

sight (BLOS) propagation, it simultaneously creates shadow zones and clutter[1-3], rendering standard radar and communication models ineffective.

Given these profound propagation effects, ADs have become a critical factor in maritime strategy and defense operations. The ability to predict these "blind zones" or "extended ranges" is often decisive in modern electronic warfare. A striking example is the April 2022 sinking of the cruiser Moskva; while the full tactical picture is complex, analyses suggest that anomalous ducting conditions may have facilitated the unexpected BLOS engagement by Neptune missiles, underscoring the operational risks of overlooking atmospheric refractivity[4]. Such high-stakes incidents highlight the imperative to understand AD dynamics, prompting significant investment in observational research.

To address these operational challenges, the scientific community has launched major field campaigns since the early 2000s focused on the formation mechanisms and predictive modeling of ADs. Prominent initiatives include Wallops-2000[5], the Rough Evaporative Duct Experiment (RED)[6], the Tropical Air-Sea Propagation Study (TAPS)[7], and the Coupled Air-Sea Processes and Electromagnetic Ducting Research (CASPER)[8]. These efforts have significantly refined the understanding of air-sea interaction parameterizations and improved the validation between refractivity structures and propagation models. However, these studies have predominantly focused on short-term process studies or seasonal statistics, leaving the broader climatic context largely unexplored.

Recently, increasingly frequent reports of anomalous propagation and radar interference globally raise a critical question: Is the baseline state of the ADs shifting? Since AD formation is physically governed by near-surface thermodynamic structure, continuous warming-driven changes in temperature and humidity profiles[9-11] are likely altering AD patterns. Here, we bridge this knowledge gap by quantifying secular trends in AD characteristics and disentangling the signal of long-term climate change from the noise of interannual variability, such as the El Niño–Southern Oscillation (ENSO)[12-15].

2 Results

2.1 Warming-driven changes in atmospheric ducts: evolution and mechanisms

Figure 1 summarizes global changes of ADs characteristics from 1979 to 2024. Over the mid- to low-latitude oceans (60°S–60°N), AD occurrence probability (Figure 1a, b, m, p), top height (Figure 1e, f, n, q), and strength (Figure 1i, j, o, r) show widespread and significant increases. Over land, AD occurrence probability and strength also grow, with the greatest positive changes in South America. In contrast, AD characteristics decline markedly over the high-latitude Southern Ocean and the Antarctic continent

How do these changes relate to warming-driven shifts in the atmospheric environment? Because AD formation is tightly linked to lower-tropospheric stability, the increases in AD occurrence probability and strength are consistent with warming-induced changes in the environmental temperature lapse rate[16-21]. The dry-adiabatic lapse rate is temperature-independent; therefore, warming-driven changes in the environmental lapse rate largely reflect a reduced moist-adiabatic lapse rate. Over humid oceans, vertical mixing more closely follows moist-adiabatic processes, increasing static stability and favouring AD formation and intensification. Over land, the boundary layer is typically drier and the moist-adiabatic lapse rate is less sensitive to warming, so mixing remains closer to dry-adiabatic and stability changes are smaller. Over Antarctica, strong stratification in the cold, dry atmosphere suppresses convection and turbulent mixing, limiting vertical heat export. Preferential near-surface warming then weakens the inversion and reduces lower-tropospheric static stability. Multi-model ensembles similarly show a marked weakening of the Antarctic inversion under high-emission scenarios[22], consistent with our results.

However, the above analysis cannot explain the increase in AD top height. Elevated ducts typically form near the top of the atmospheric boundary layer, and their height is therefore closely related to boundary-layer depth[23]. Because stable boundary layers are generally shallower[24], a stability-only argument would instead imply a decrease in AD top height. Boundary-layer depth, however, is jointly controlled by entrainment at the boundary-layer top and the large-scale vertical motion[25]. Although stability tends to suppress entrainment, global warming has been reported to weaken the equatorial large-scale circulation, thereby altering the background vertical velocity[26,27]. Since ADs preferentially occur in large-scale subsidence regimes, weakened subsidence can lift the boundary laye[28] and increase AD top height.

Compared to changes in annual-mean characteristics, the annual standard deviation of AD features varies little over time across most regions. This suggests that long-term changes in the seasonal variability of AD characteristics are relatively gradual. However, in most oceanic regions, the annual standard deviation of AD occurrence probability and strength exhibits a coherent positive trend (Figure 1d, l). Under global warming, seasonal variability in precipitation is reported to increase [29-32], manifesting as wetter wet seasons and drier dry seasons. Oceanic areas remain highly humid near surface, and precipitation affects mid-level atmospheric moisture more strongly than the boundary layer[33]. During the wet season, mid-level moistening reduces vertical humidity gradients, thereby decreasing the occurrence probability and strength of ADs. Conversely, during the dry season, mid-level drying increases vertical humidity gradients, enhancing the occurrence probability and strength of ADs. Consequently, the seasonal variability of ADs intensifies. Over the Antarctic continent, the annual standard deviation of AD occurrence probability and strength shows a consistent decreasing trend (Figure 1d, l). This is consistent with the seasonal cycle of the inversion layer[22], which becomes stronger in Antarctic winters and weaker in summers due to radiative cooling[34]. Under global warming, lower-atmospheric warming over Antarctica is reported to be faster in winter than in summer[35], leading to a more rapid decline in stability. This reduces the occurrence probability and strength of ADs while also weakening their seasonal variability.

The above physical mechanism analysis indicates that change of atmospheric environmental under global warming may be the primary driver of long-term AD evolution. To statistically validate this conclusion, the relationship between AD EOF modes and global-mean temperature was examined. The analysis shows that, when the long-term trend is retained, the leading EOF mode of ADs is significantly and positively correlated with the global-mean 2 m air temperature (Figure 2); once the long-term trend is removed, this correlation weakens markedly or even disappears (Supporting Information 1 Figure S1). Given that the leading modes are concentrated over oceanic regions, similar work was done to mean sea surface temperature (SST), and obtained results consistent with those based on global-mean 2 m air temperature (Supporting Information 1 Figures S2–S3). The influence was further quantified through EOF mode reconstruction. For AD occurrence probability (Supporting Information 2 Figures S1–S4), after excluding summer (owing to strong coupling between ENSO and the global-warming mode), the third mode in spring dominated by global warming, together with the second modes in autumn and winter, exhibits significant increasing trends. The magnitude

of this increase is consistent with the changes shown in Figure 1. Similarly, AD strength (Supporting Information 3 Figures S1–S4) and top height (Supporting Information 4 Figures S1–S4) show analogous behaviour, with global warming often exceeding ENSO as the dominant influence in the leading AD mode. Collectively, these results support the conclusion that atmospheric environmental changes closely linked to global warming drive the long-term trends in ADs.

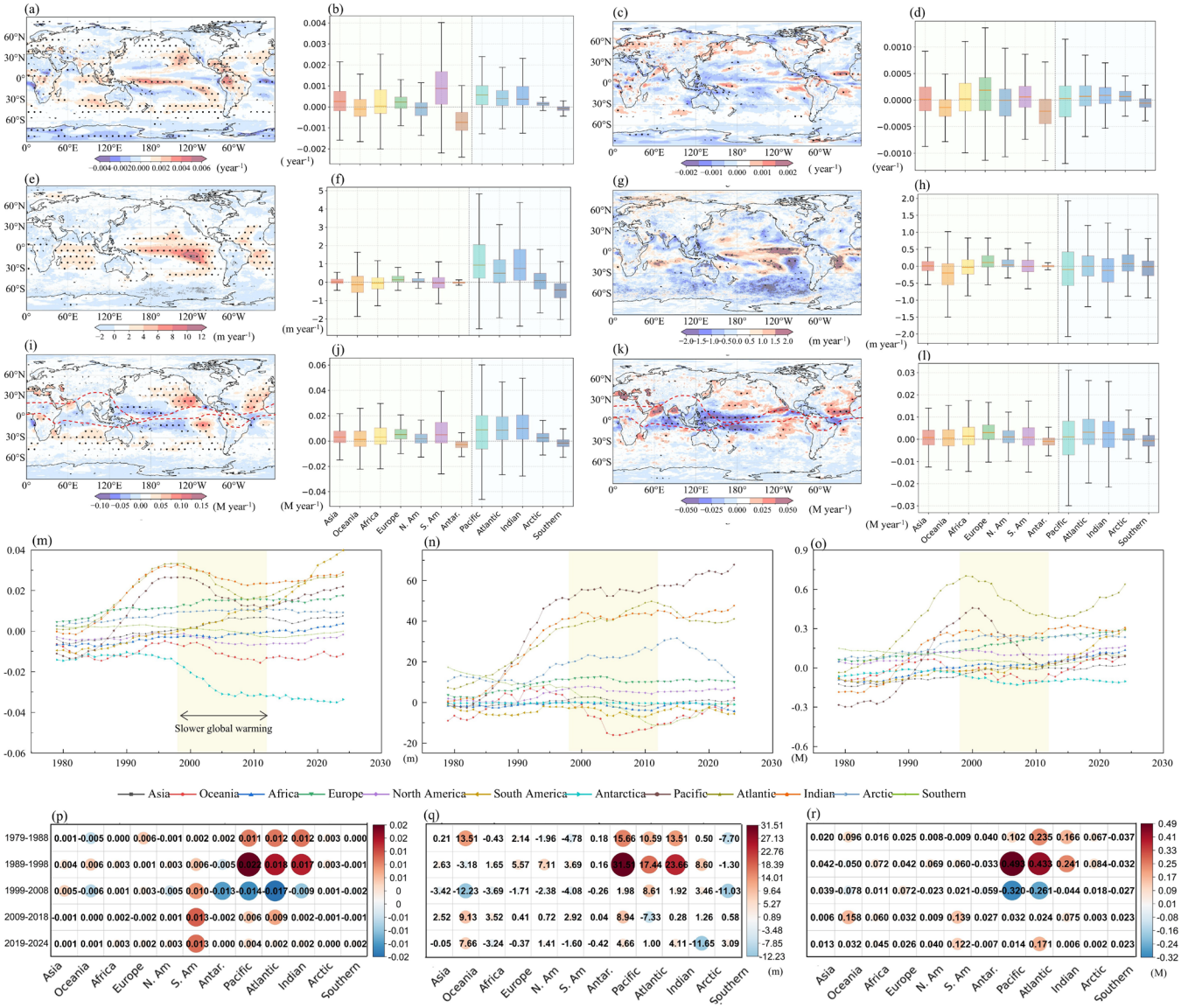

Figure 1 Long-term changes in atmospheric duct (AD) characteristics from 1979 to 2024.

Column 1 (rows 1–3) shows trends in the annual-mean AD occurrence probability, top height, and strength. Column 3 (rows 1–3) shows trends in the annual standard deviation of these AD characteristics. Trends are estimated using linear regression of each AD metric against time. Columns 2 and 4 summarize the corresponding trend statistics for major oceanic and continental regions. Row 4 shows changes in AD characteristics relative to 1979, smoothed with a 10-year running mean. Row 5 shows the endpoint 10-year change, defined as X(end) − X(start) for each 10-year window. Shaded areas indicate trends significant at the 95% confidence level (t-test). Red dashed lines in subfigures i and k mark the equatorial convergence zone.

2.2 Modulation of long-term atmospheric duct evolution by dominant climate modes

Beyond global warming, major climate modes—particularly ENSO—significantly modulate AD evolution (Figure 2). This likely explains the spatial contrast between the widespread AD strengthening over mid-to-low latitude oceans and the localized weakening in the western Pacific (Figure 1). Regionally averaged AD characteristics (30°S–30°N; Supporting Information 1 Figure S4) display a non-monotonic trend: an initial increase followed by a decline, rather than a continuous decrease. This decline coincides with the "global warming hiatus, "[36] where AD growth stalled (Supporting Information 2-4 Figures S1–4) alongside sustained La Niña conditions. Theoretically, La Niña shifts convection westward, enhancing precipitation and reducing vertical humidity gradients in the western Pacific. This mechanism suppresses AD probability and strength, yielding the negative trends observed in Figure 1a, i. Concurrently, an intensified Hadley circulation limits AD top height growth in subsidence zones. Sensitivity analysis confirms that AD responses to ENSO are concentrated in low latitudes (Supporting Information 1 Figure S5). Modal reconstruction further validates that this ENSO-dominated mode drove the observed AD decline, peaking in winter. However, given ENSO's high-frequency variability, its contribution to the long-term AD trend remains negligible.

Wavelet analysis reveals a third, lower-frequency mode of AD variability, subordinate only to global warming and ENSO. Spatially, this mode exhibits high sign consistency across mid-to-low latitude oceans, centering on the central-eastern equatorial Pacific (Supporting Information 2-4 Figures S1–S4). Reconstructions indicate a sustained AD increase from 1979 to 1998, followed by a sharp post-1998 decline and subsequent

stabilization. While coincident with various climate shifts, it is difficult to attribute this global pattern to any single physical signal. This may be related to the changes in data assimilation of ERA5. Hersbach, et al. [37] noted that, since the 1980s, the introduction of Microwave Imagers has led to a tendency for the middle atmosphere to be warmer and drier, which effectively explains the enhancement of ADs before 1998 in this mode. Furthermore, their study mentioned that the introduction of the Advanced Microwave Sounding Unit (AMSU) resulted in a global shift in ERA5 precipitation around the year 2000, followed by a period of relative stability, which may have contributed to the weakening of the ADs after 1998.

Figure 2 Partial correlation analysis between EOF principal component of AD characteristics and major climate factors. Seasons are defined as DJF (winter), MAM (spring), JJA (summer), and SON (autumn). Climate factors include AAO (Antarctic Oscillation), AO (Arctic Oscillation), ENSO (El Niño–Southern Oscillation), IOD (Indian Ocean Dipole), MJO (Madden–Julian Oscillation), NAO (North Atlantic Oscillation), PDO (Pacific Decadal Oscillation), and t2m (2 m air temperature). Asterisks (*) denote values significant at the 95% confidence level (t-test).

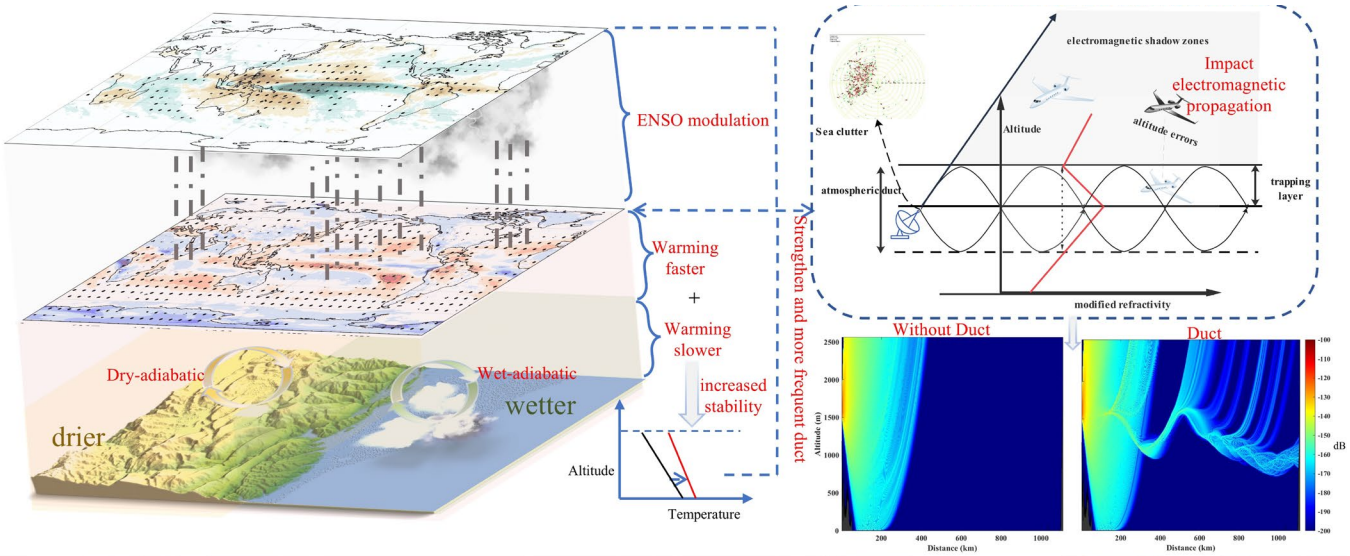

Figure 3 Mechanisms linking global warming, ADs, and electromagnetic propagation

3 Conclusion

This study establishes the first physical link between AD evolution and global climate change. We identify a significant strengthening of mid-to-low latitude oceanic ADs since 1979. This long-term evolution is governed primarily by increased atmospheric stability driven by global warming, rather than by natural variability. While ENSO modulates short-term interannual oscillations, global warming acts as the dominant driver, systematically reshaping the electromagnetic propagation environment of the global atmosphere.

Acknowledgements. ERA5 reanalysis data were obtained from the Copernicus Climate Change Service Climate Data Store. We thank the scientists, engineers, and data managers who developed and maintain this dataset.

References

1 Mcpetrie, J. S. & Starnecki, B. Low-Level Atmospheric Ducts. *Nature* **162**, 818-818, doi:10.1038/162818a0 (1948).

2 Bean, B. R. & Dutton, E. J. *Radio Meteorology.* 1-21 (Dover, 1968).

3 Battan, L. J. Radar Observation of the Atmosphere. *Quarterly Journal of the Royal Meteorological Society* **99**, 793-793, doi:10.1002/qj.49709942229 (1973).

4 Norin, L., Wellander, N. & Devasthale, A. Anomalous Propagation and the Sinking of the Russian Warship Moskva. *Bulletin of the American Meteorological Society* **104**,

E2286-E2304, doi:https://doi.org/10.1175/BAMS-D-23-0113.1 (2023).

5 Thompson, W. T. & Haack, T. An Investigation of Sea Surface Temperature Influence on Microwave Refractivity: The Wallops-2000 Experiment. *Journal of Applied Meteorology and Climatology* **50**, 2319-2337, doi:https://doi.org/10.1175/JAMC-D-10-05002.1 (2011).

6 Anderson, K. *et al.* The Red Experiment: An Assessment of Boundary Layer Effects in a Trade Winds Regime on Microwave and Infrared Propagation over the Sea. *Bulletin of the American Meteorological Society* **85**, 1355-1366, doi:https://doi.org/10.1175/BAMS-85-9-1355 (2004).

7 Kulessa, A. S. *et al.* The Tropical Air–Sea Propagation Study (Taps). *Bulletin of the American Meteorological Society* **98**, 517-537, doi:https://doi.org/10.1175/BAMS-D-14-00284.1 (2017).

8 Wang, Q. *et al.* CASPER: Coupled Air–Sea Processes and Electromagnetic Ducting Research. *Bulletin of the American Meteorological Society* **99**, 1449-1471, doi:https://doi.org/10.1175/BAMS-D-16-0046.1 (2018).

9 Cook, B. I. *et al.* Twenty-First Century Drought Projections in the CMIP6 Forcing Scenarios. *Earth's Future* **8**, e2019EF001461, doi:https://doi.org/10.1029/2019EF001461 (2020).

10 Domeisen, D. I. V. *et al.* Prediction and Projection of Heatwaves. *Nature Reviews Earth & Environment* **4**, 36-50, doi:10.1038/s43017-022-00371-z (2023).

11 Grant, L. *et al.* Global Emergence of Unprecedented Lifetime Exposure to Climate Extremes. *Nature* **641**, 374-379, doi:10.1038/s41586-025-08907-1 (2025).

12 Philander, S. G. H., Yamagata, T. & Pacanowski, R. C. Unstable Air-Sea Interactions in the Tropics. *Journal of Atmospheric Sciences* **41**, 604-613, doi:https://doi.org/10.1175/1520-0469(1984)041<0604:UASIIT>2.0.CO;2 (1984).

13 Ropelewski, C. F. & Halpert, M. S. Global and Regional Scale Precipitation Patterns Associated with the El Niño/Southern Oscillation. *Monthly Weather Review* **115**, 1606-1626, doi:https://doi.org/10.1175/1520-0493(1987)115<1606:GARSPP>2.0.CO;2 (1987).

14 Mcphaden, M. J., Zebiak, S. E. & Glantz, M. H. Enso as an Integrating Concept in Earth Science. *Science* **314**, 1740-1745, doi:doi:10.1126/science.1132588 (2006).

15 Geng, T. *et al.* Increased Occurrences of Consecutive La Niña Events under Global Warming. *Nature* **619**, 774-781, doi:10.1038/s41586-023-06236-9 (2023).

16 Joshi, M. M., Gregory, J. M., Webb, M. J., Sexton, D. M. H. & Johns, T. C. Mechanisms for the Land/Sea Warming Contrast Exhibited by Simulations of Climate

Change. *Climate Dynamics* **30**, 455-465, doi:10.1007/s00382-007-0306-1 (2008).

17 Fasullo, J. T. Robust Land–Ocean Contrasts in Energy and Water Cycle Feedbacks. *Journal of Climate* **23**, 4677-4693, doi:10.1175/2010jcli3451.1 (2010).

18 Byrne, M. P. & O'gorman, P. A. Land–Ocean Warming Contrast over a Wide Range of Climates: Convective Quasi-Equilibrium Theory and Idealized Simulations. *Journal of Climate* **26**, 4000-4016, doi:https://doi.org/10.1175/JCLI-D-12-00262.1 (2013).

19 Byrne, M. P. & O'gorman, P. A. Trends in Continental Temperature and Humidity Directly Linked to Ocean Warming. *Proceedings of the National Academy of Sciences* **115**, 4863-4868, doi:doi:10.1073/pnas.1722312115 (2018).

20 Brogli, R. *et al.* Future Summer Warming Pattern under Climate Change Is Affected by Lapse-Rate Changes. *Weather and Climate Dynamics* **2**, 1093-1110, doi:10.5194/wcd-2-1093-2021 (2021).

21 Wang, Z., Jing, Z. & Song, F. Weakened Large-Scale Surface Heat Flux Feedback at Midlatitudes under Global Warming. *Nature Communications* **15**, 10020, doi:10.1038/s41467-024-54394-9 (2024).

22 Ding, M. *et al.* On the Shallowing of Antarctic Low-Level Temperature Inversions Projected by Cesm-Le under Rcp8.5. *Journal of Meteorological Research* **38**, 586-599, doi:10.1007/s13351-024-3146-6 (2024).

23 Engeln, V. & Axel. A Ducting Climatology Derived from the European Centre for Medium-Range Weather Forecasts Global Analysis Fields. *Journal of Geophysical Research: Atmospheres* **109**, doi:10.1029/2003JD004380 (2004).

24 Huang, J. & Bou-Zeid, E. Turbulence and Vertical Fluxes in the Stable Atmospheric Boundary Layer. Part I: A Large-Eddy Simulation Study. *Journal of the Atmospheric Sciences* **70**, 1513-1527, doi:https://doi.org/10.1175/JAS-D-12-0167.1 (2013).

25 Stevens, B. Entrainment in Stratocumulus-Topped Mixed Layers. *Quarterly Journal of the Royal Meteorological Society* **128**, 2663-2690, doi:https://doi.org/10.1256/qj.01.202 (2002).

26 Vecchi, G. A. & Soden, B. J. Global Warming and the Weakening of the Tropical Circulation. *Journal of Climate* **20**, 4316-4340, doi:https://doi.org/10.1175/JCLI4258.1 (2007).

27 Kjellsson, J. Weakening of the Global Atmospheric Circulation with Global Warming. *Climate Dynamics* **45**, 975-988, doi:10.1007/s00382-014-2337-8 (2015).

28 Blossey, P. N. *et al.* Marine Low Cloud Sensitivity to an Idealized Climate Change: The Cgils Les Intercomparison. *Journal of Advances in Modeling Earth Systems* **5**, 234-258,

doi:https://doi.org/10.1002/jame.20025 (2013).

29 Chou, C. & Lo, M.-H. Asymmetric Responses of Tropical Precipitation During Enso. *Journal of Climate* **20**, 3411-3433, doi:https://doi.org/10.1175/JCLI4197.1 (2007).

30 Chou, C., Tu, J.-Y. & Tan, P.-H. Asymmetry of Tropical Precipitation Change under Global Warming. *Geophysical Research Letters* **34**, doi:https://doi.org/10.1029/2007GL030327 (2007).

31 Tan, P. H., Chou, C. & Tu, J. Y. Mechanisms of Global Warming Impacts on Robustness of Tropical Precipitation Asymmetry. *Journal of Climate* **21**, 5585-5602 (2008).

32 Chou, C. & Lan, C.-W. Changes in the Annual Range of Precipitation under Global Warming. *Journal of Climate* **25**, 222-235, doi:https://doi.org/10.1175/JCLI-D-11-00097.1 (2012).

33 Holloway, C. E. & Neelin, J. D. Moisture Vertical Structure, Column Water Vapor, and Tropical Deep Convection. *Journal of the Atmospheric Sciences* **66**, 1665-1683, doi:https://doi.org/10.1175/2008JAS2806.1 (2009).

34 Dice, M. J. *et al.* Forcing for Varying Boundary Layer Stability across Antarctica. *Weather and Climate Dynamics* **5**, 369-394, doi:10.5194/wcd-5-369-2024 (2024).

35 Chapman, W. L. & Walsh, J. E. A Synthesis of Antarctic Temperatures. *Journal of Climate* **20**, 4096-4117, doi:https://doi.org/10.1175/JCLI4236.1 (2007).

36 Su, X. *et al.* Reductions in Atmospheric Levels of Non-Co2 Greenhouse Gases Explain About a Quarter of the 1998-2012 Warming Slowdown. *Communications Earth & Environment* **5**, 594, doi:10.1038/s43247-024-01723-x (2024).

37 Hersbach, H. *et al.* The ERA5 Global Reanalysis. *Quarterly Journal of the Royal Meteorological Society* **146**, 1999-2049, doi:10.1002/qj.3803 (2020).

Supporting Information1

Figure S1 Partial correlations between the EOF principal components (PCs) of detrended atmospheric duct (AD) characteristics and major climate indices. Seasons are defined as DJF (winter), MAM (spring), JJA (summer), and SON (autumn). Climate factors include AAO (Antarctic Oscillation), AO (Arctic Oscillation), ENSO (El Niño–Southern Oscillation), IOD (Indian Ocean Dipole), MJO (Madden–Julian Oscillation), NAO (North Atlantic Oscillation), PDO (Pacific Decadal Oscillation), and t2m (2 m air temperature). Asterisks (*) denote values significant at the 95% confidence level (t-test).

Figure S2 Same as Figure 2, but with t2m replaced by global mean sea surface temperature (SST).

Figure S3 Same as Figure S2, but with the long-term trend removed.

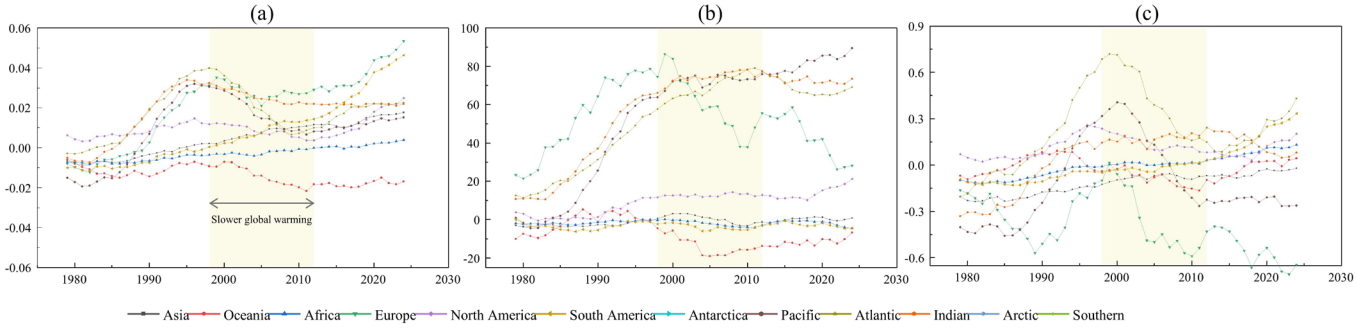

Figure S4 10-year running mean time series of AD characteristics for different regions over 30°S-30°N.

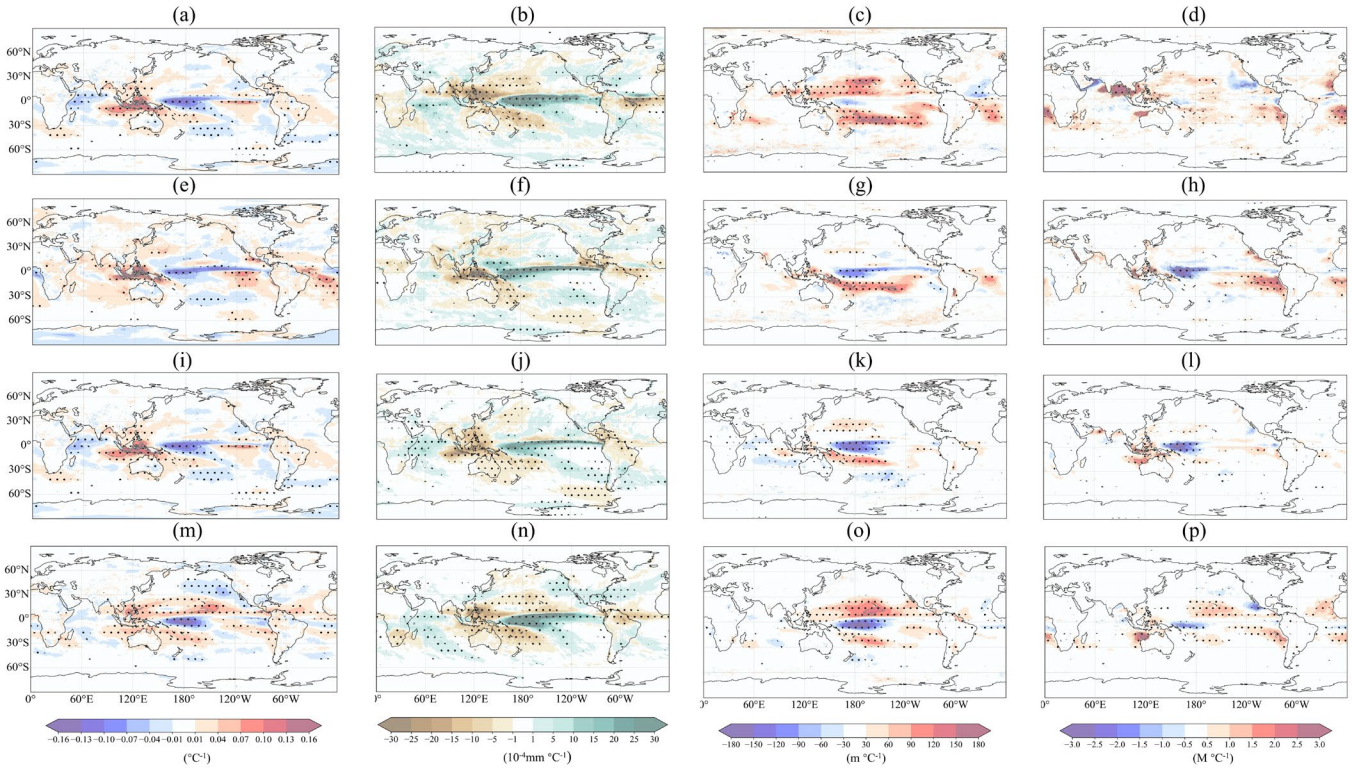

Figure S5 Spatial distributions of the regression coefficients of monthly mean AD characteristics onto the Niño-3.4 index. Columns 1, 3, and 4 display the results for AD occurrence probability, top height, and strength, respectively. Column 2 shows the results for precipitation ($\times 10^4$). Rows 1–4 correspond to the four seasons: spring, summer, autumn, and winter, respectively. Shading indicates regions with statistical significance at the 95% confidence level (Student's t-test).

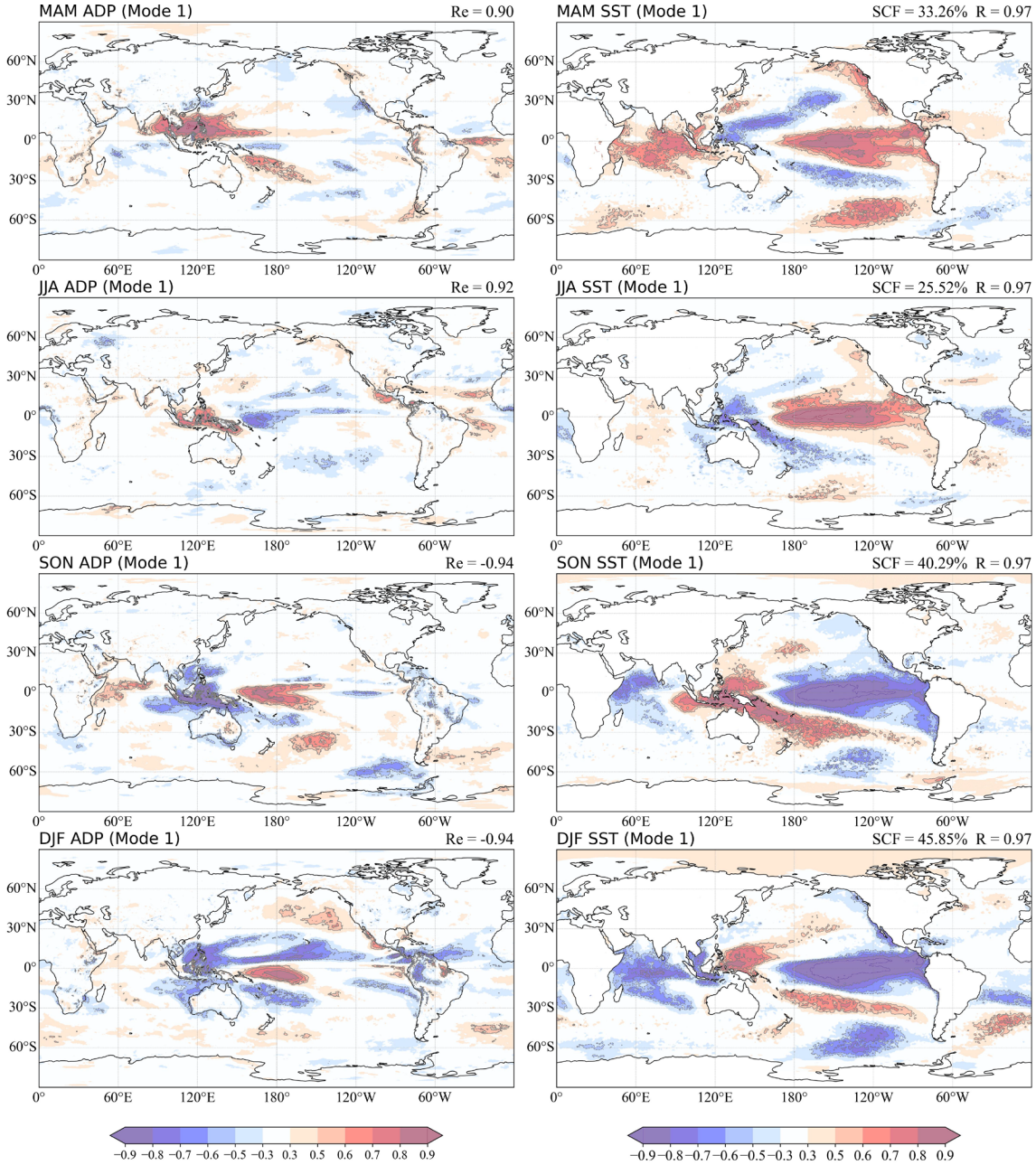

Figure S6 Maximum covariance analysis (MCA) between monthly mean AD characteristics and SST. The results are displayed as the correlation coefficients between the original field of one variable and the principal component (PC) of the other. Columns 1 and 2 display the first coupled mode for atmospheric duct characteristics and SST, respectively. Rows 1–4 correspond to the four seasons: spring, summer, autumn, and winter, respectively. Re represents the correlation coefficient between the PC and the Niño-3.4 index. SCF indicates the squared covariance fraction, representing the proportion of the covariability explained by the first mode. R is the correlation coefficient

between the PCs of the two variables.

Supporting Information2

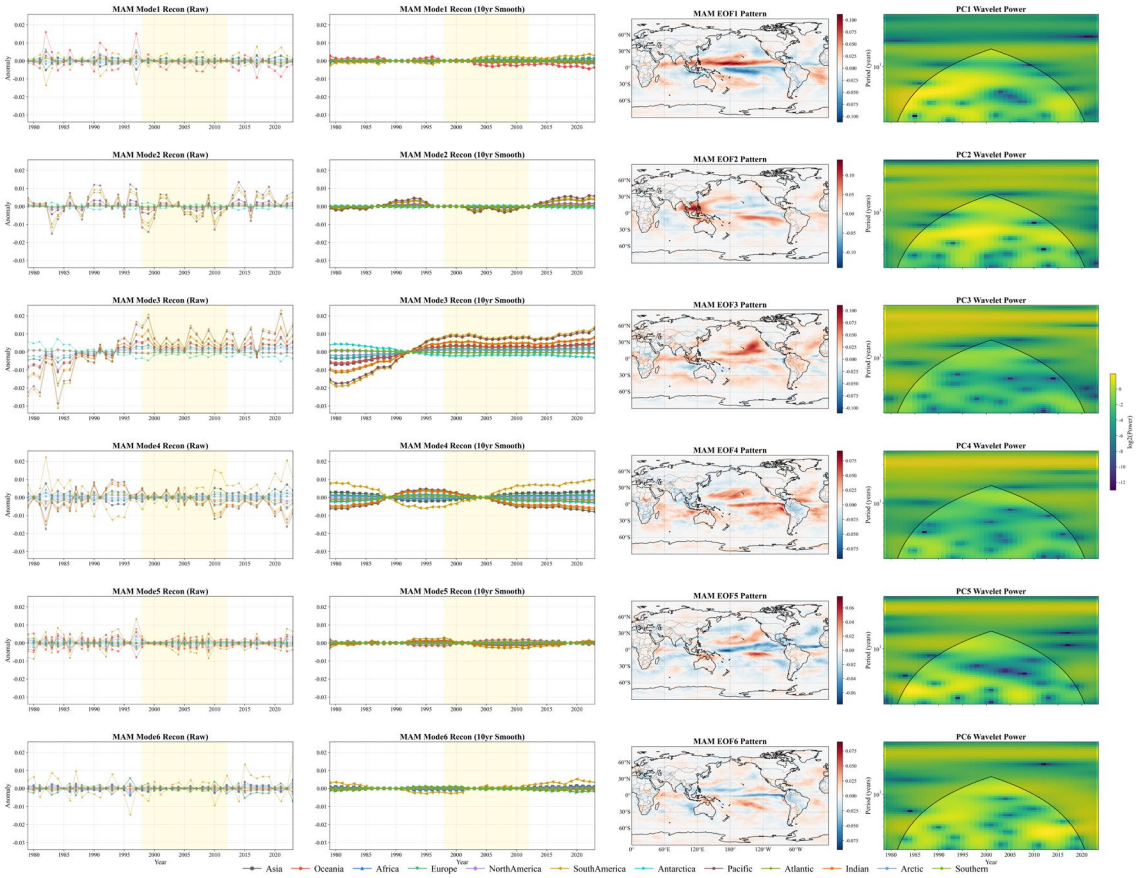

Figure S1 Reconstructions based on the leading EOF modes of the atmospheric duct (AD) occurrence probability in spring. Columns 1–4 display the reconstructed fields, 10-year running means of the reconstructions, spatial patterns of the modes, and wavelet analysis of the principal components (PCs), respectively.

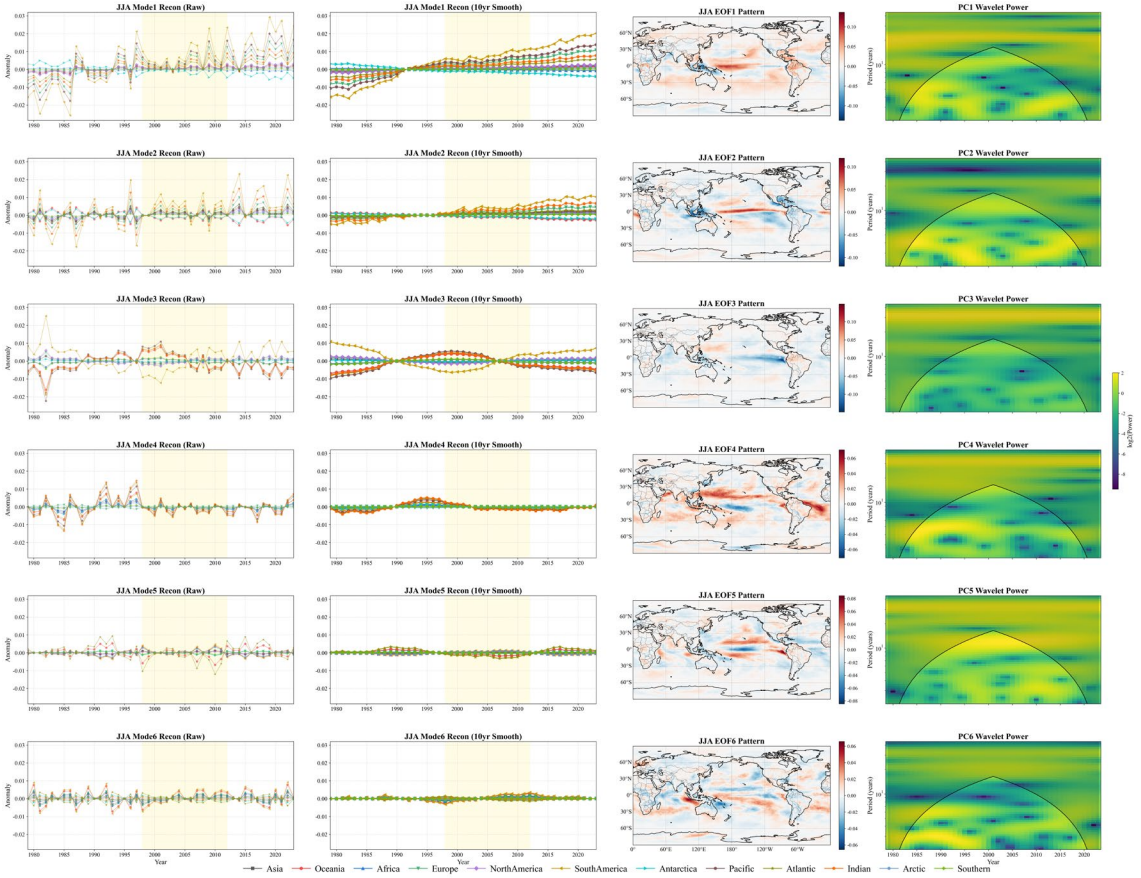

Figure S2 Same as Figure S1, but for summer.

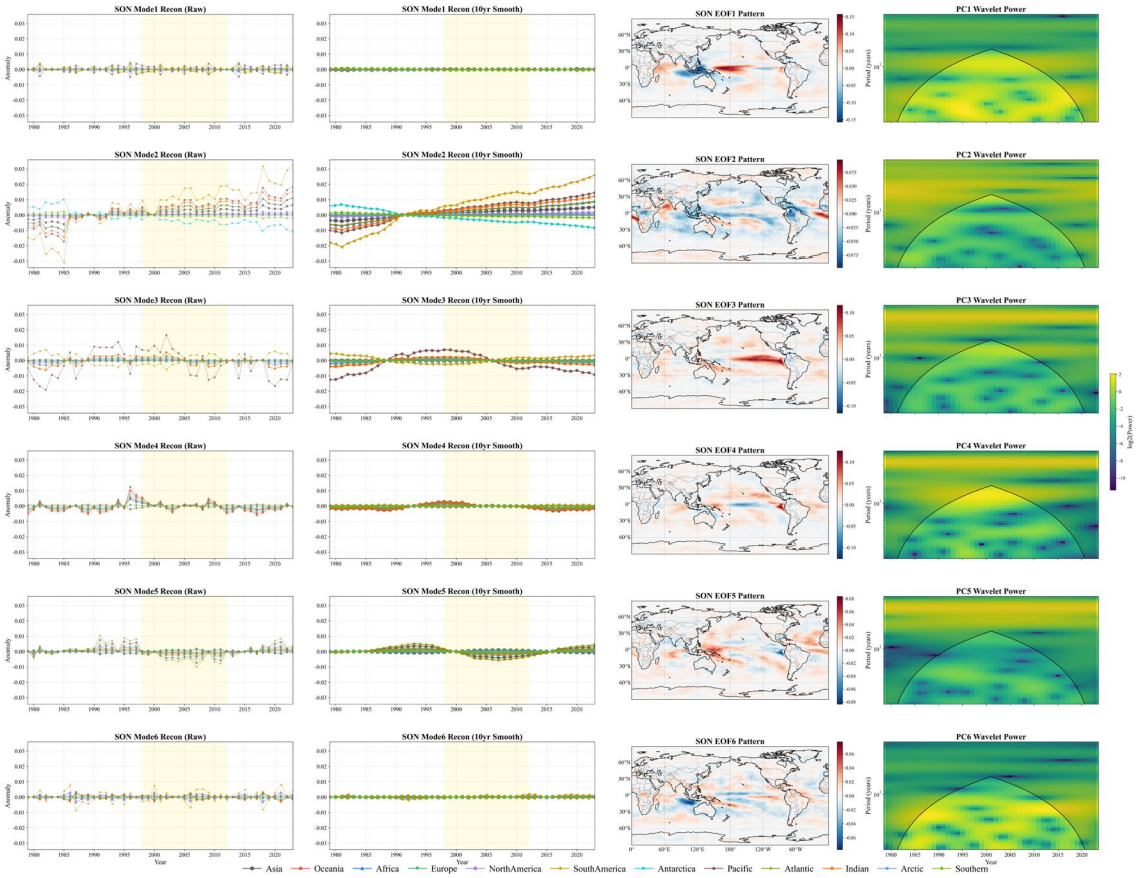

Figure S3 Same as Figure S1, but for autumn.

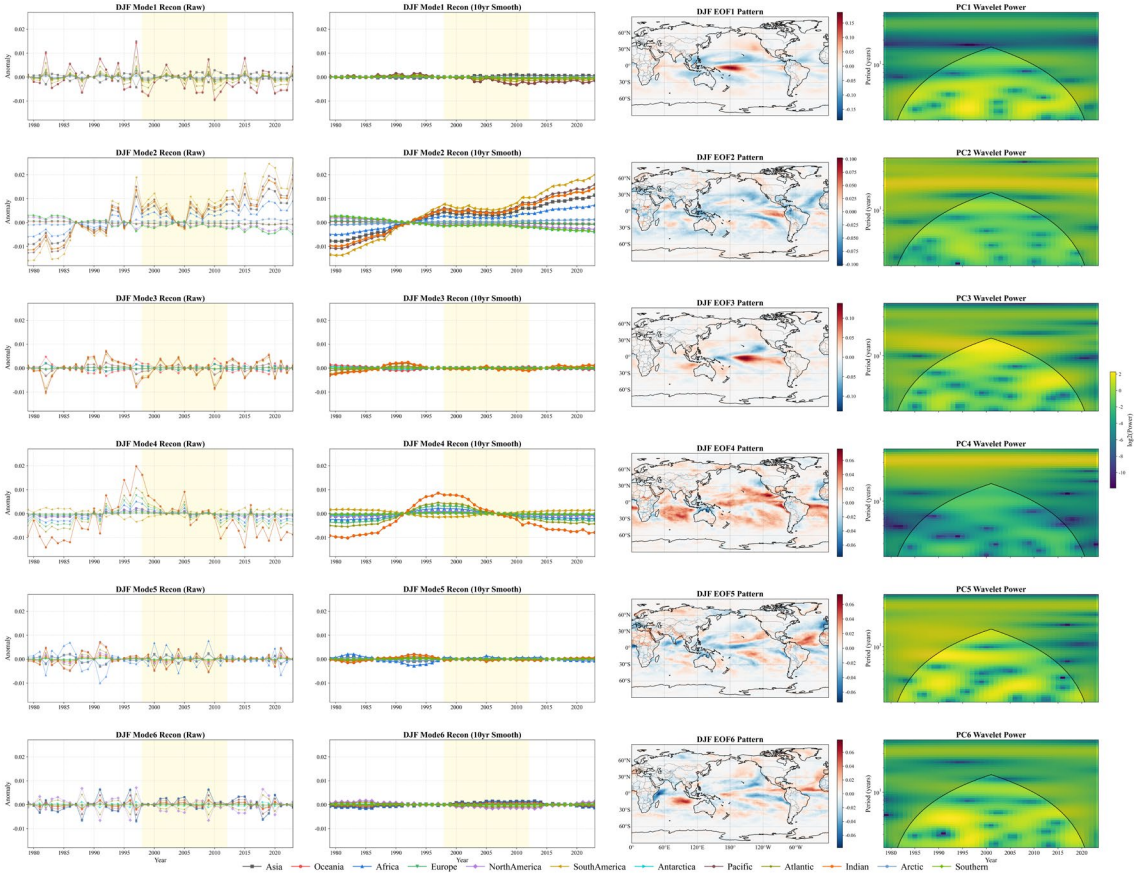

Figure S4 Same as Figure S1, but for winter.

Supporting Information3

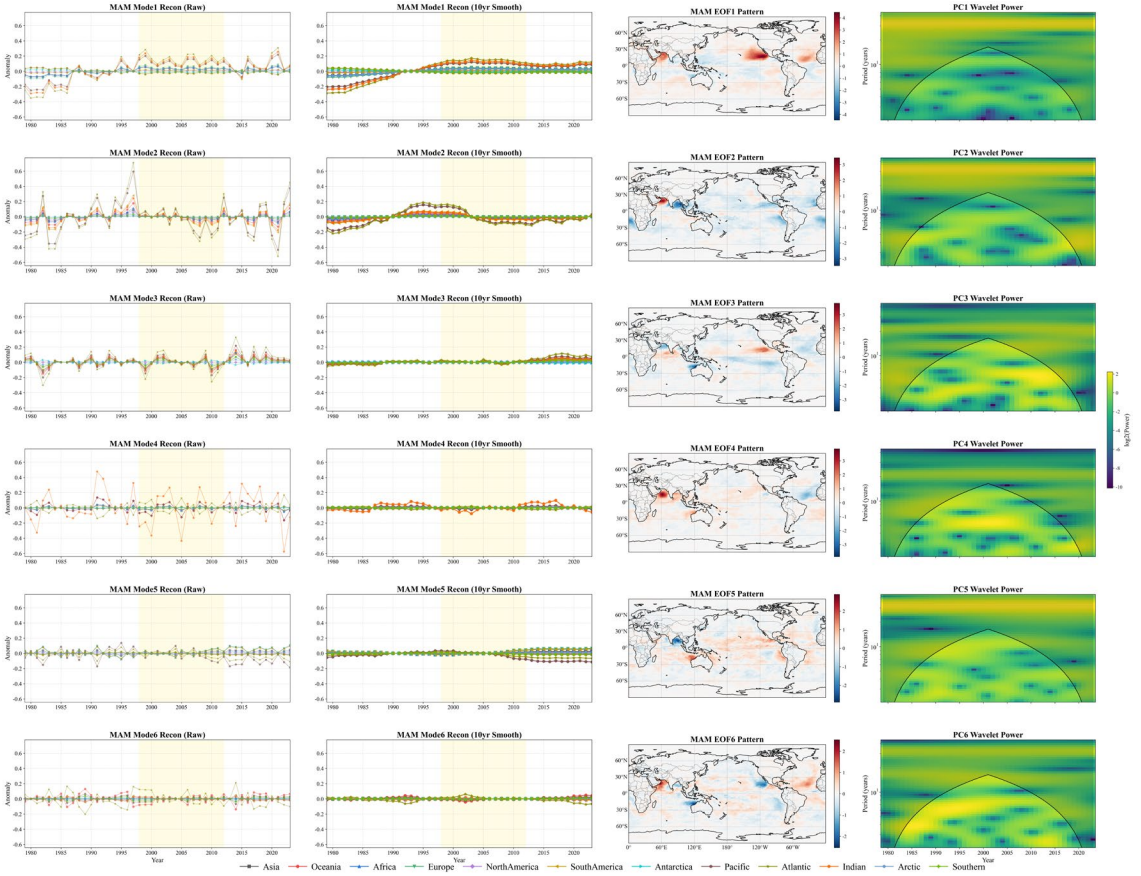

Figure S1 Reconstructions based on the leading EOF modes of the atmospheric duct (AD) strength in spring. Columns 1–4 display the reconstructed fields, 10-year running means of the reconstructions, spatial patterns of the modes, and wavelet analysis of the principal components (PCs), respectively.

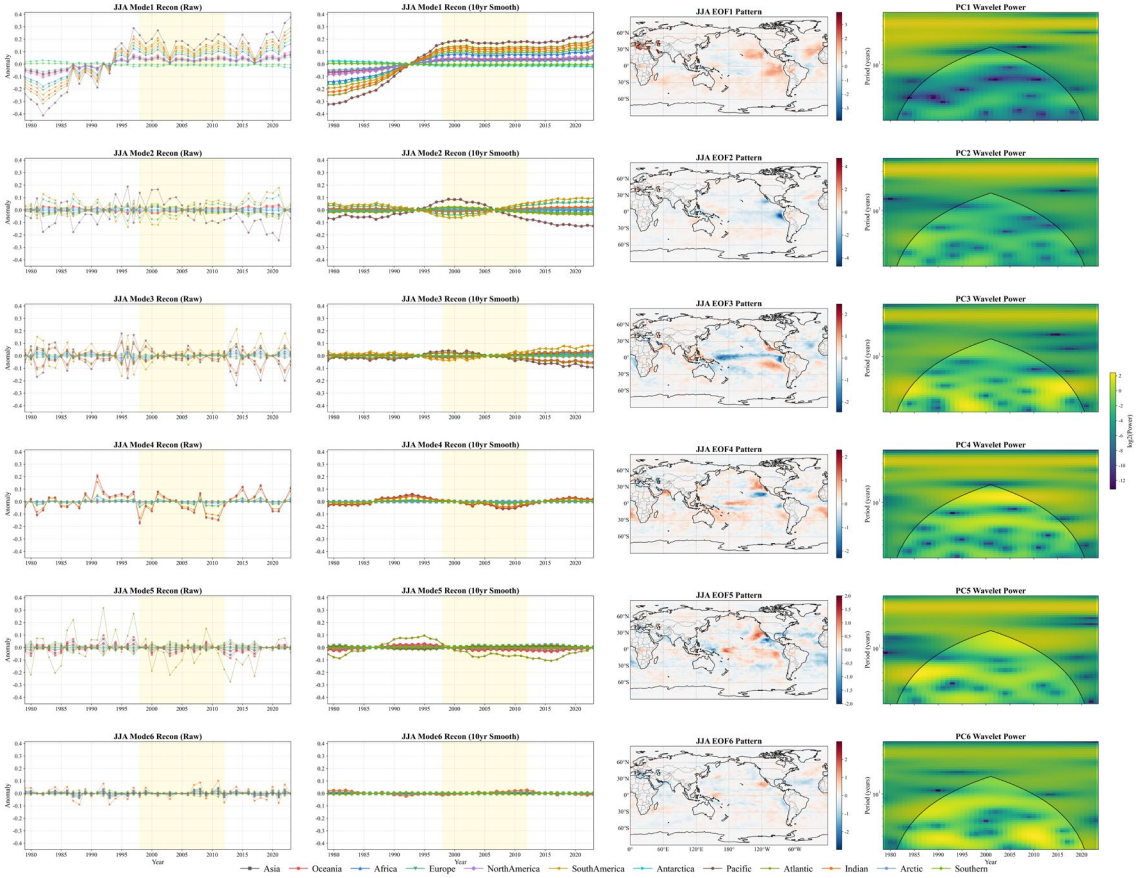

Figure S2 Same as Figure S1, but for summer.

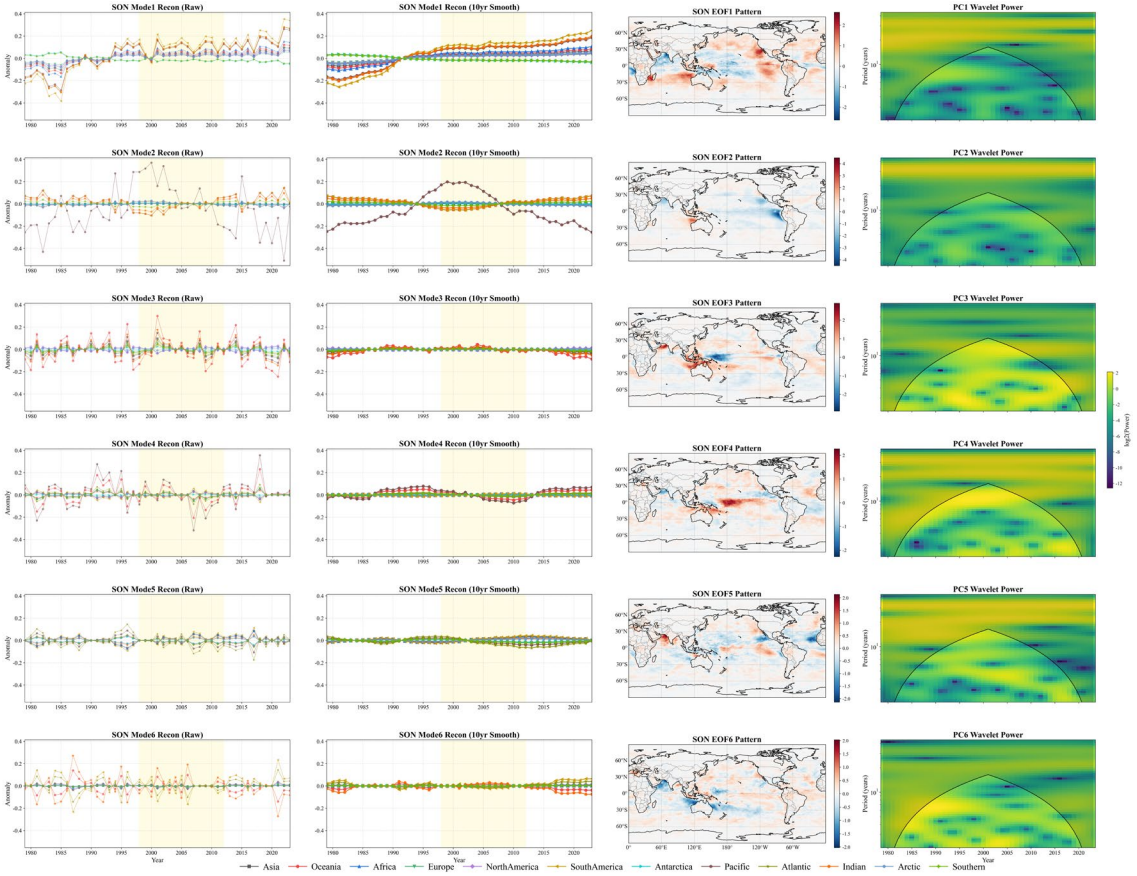

Figure S3 Same as Figure S1, but for autumn.

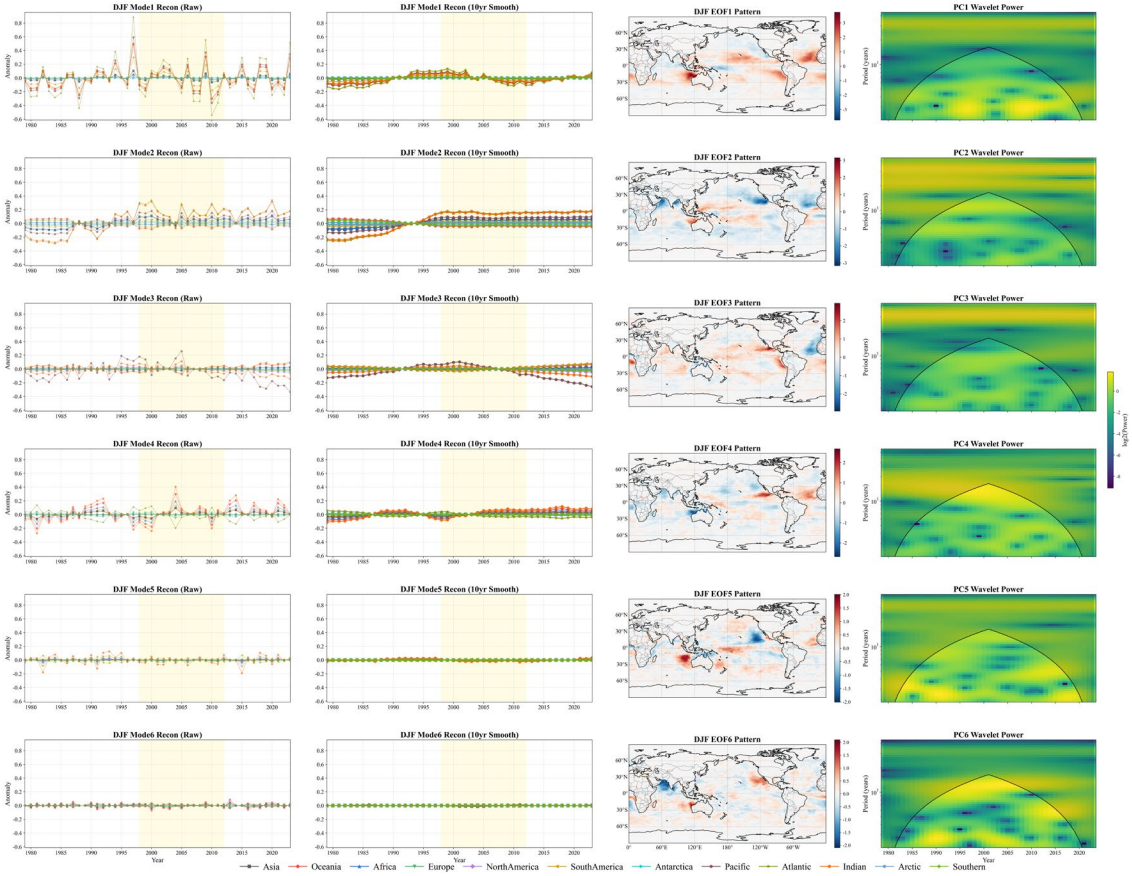

Figure S4 Same as Figure S1, but for winter.

Supporting Information4

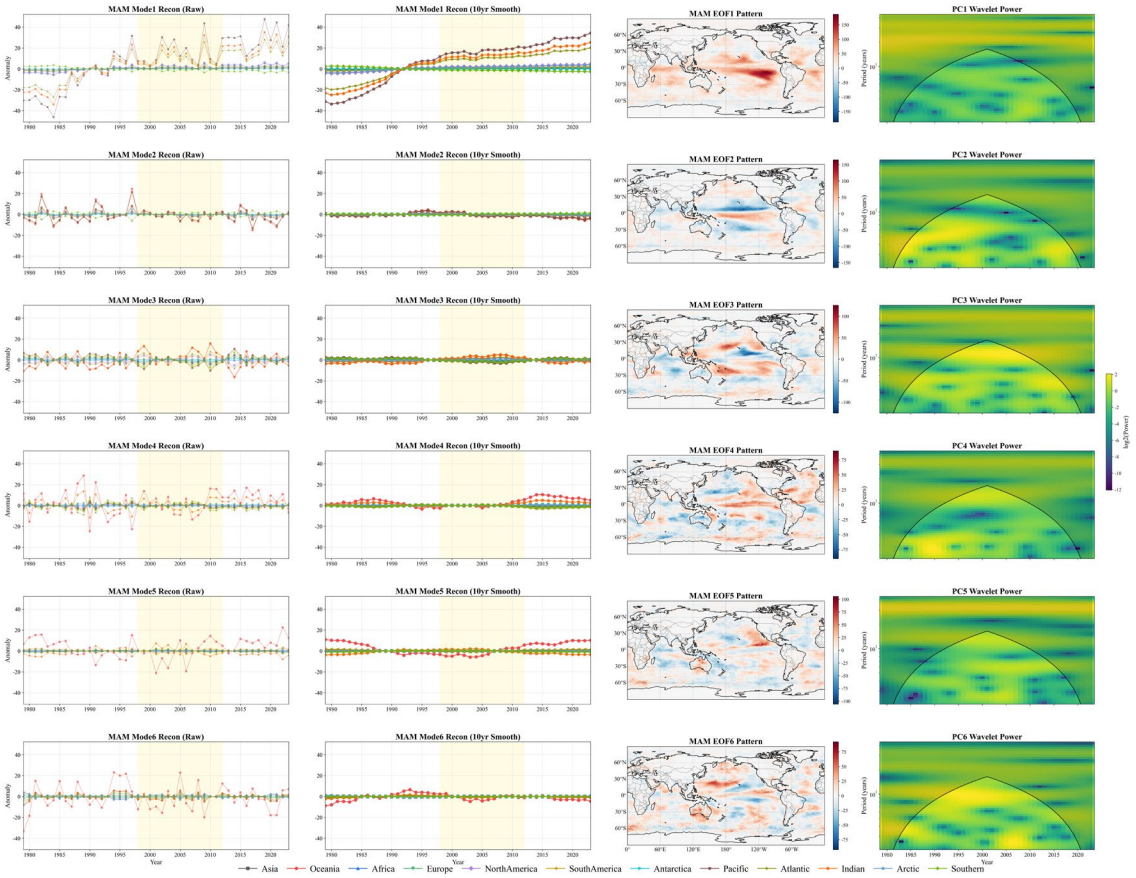

Figure S1 Reconstructions based on the leading EOF modes of the atmospheric duct (AD) top height in spring. Columns 1–4 display the reconstructed fields, 10-year running means of the reconstructions, spatial patterns of the modes, and wavelet analysis of the principal components (PCs), respectively.

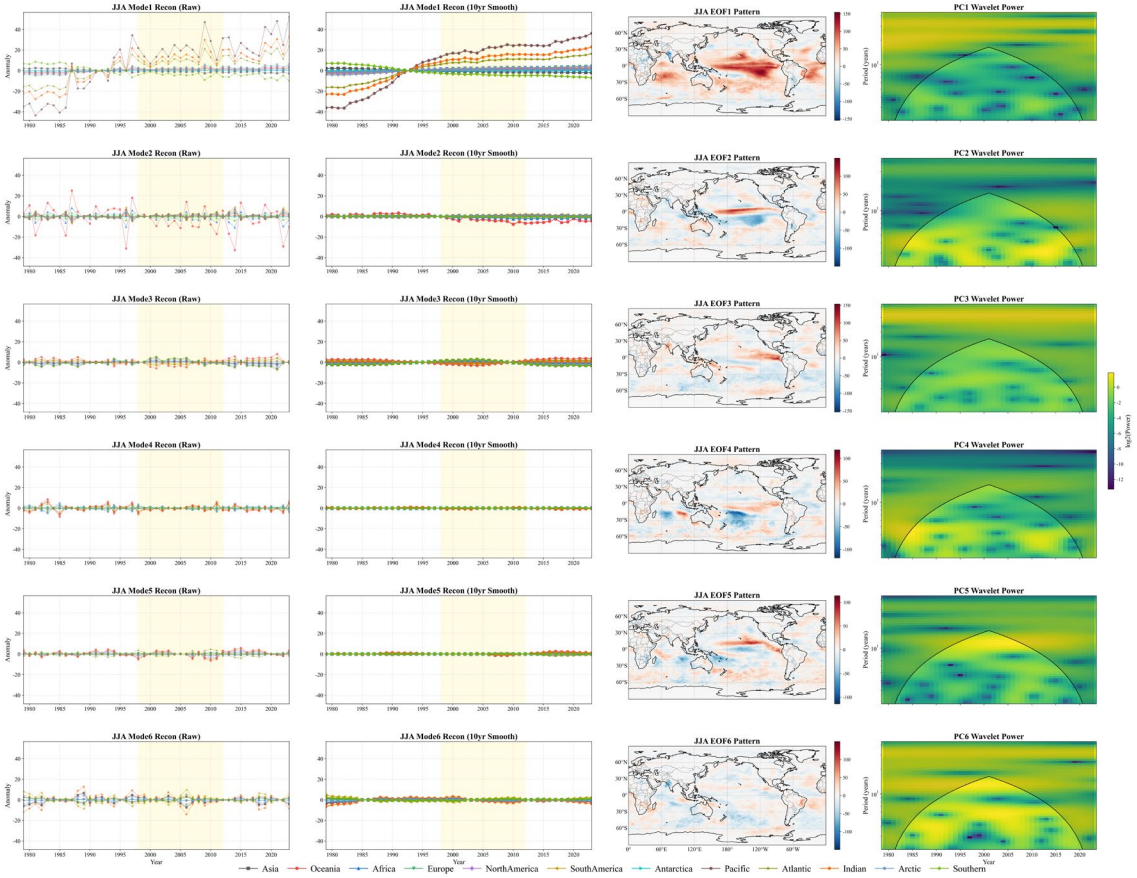

Figure S2 Figure S3 Same as Figure S1, but for summer.

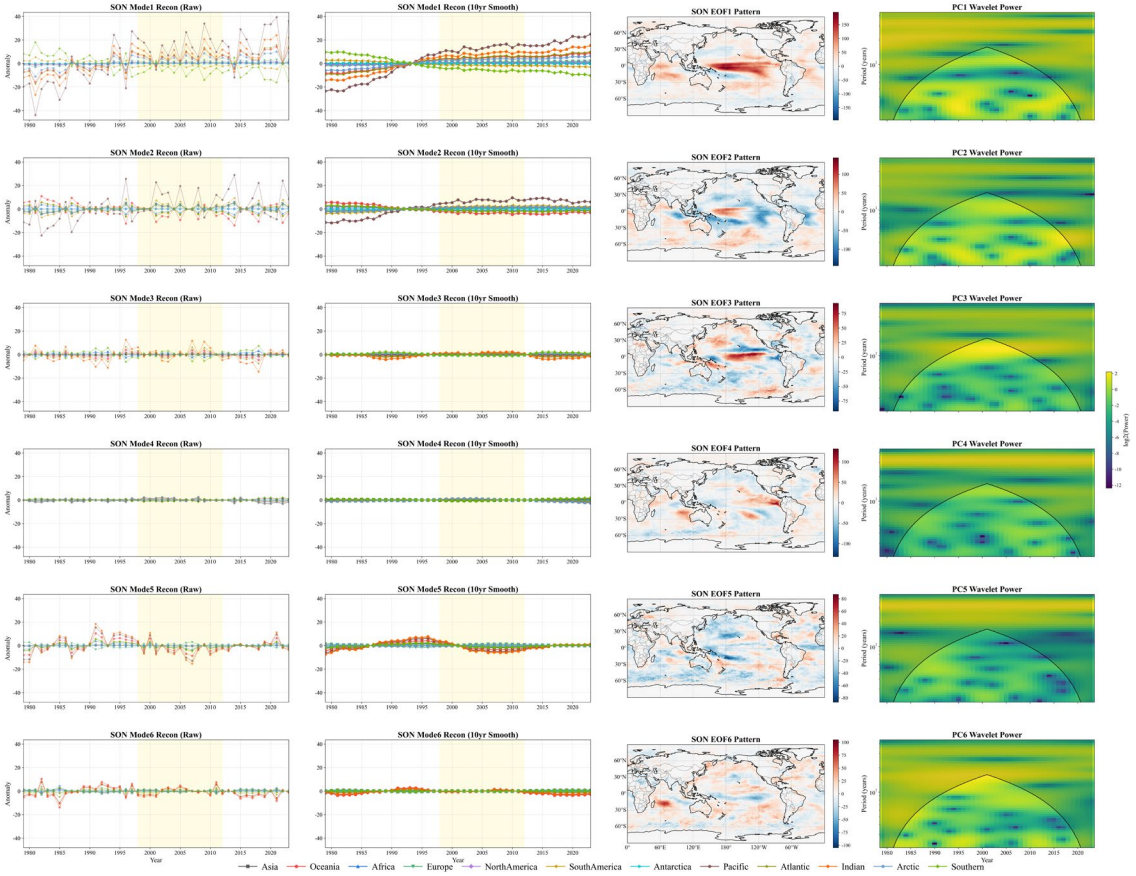

Figure S4 Same as Figure S1, but for autumn.

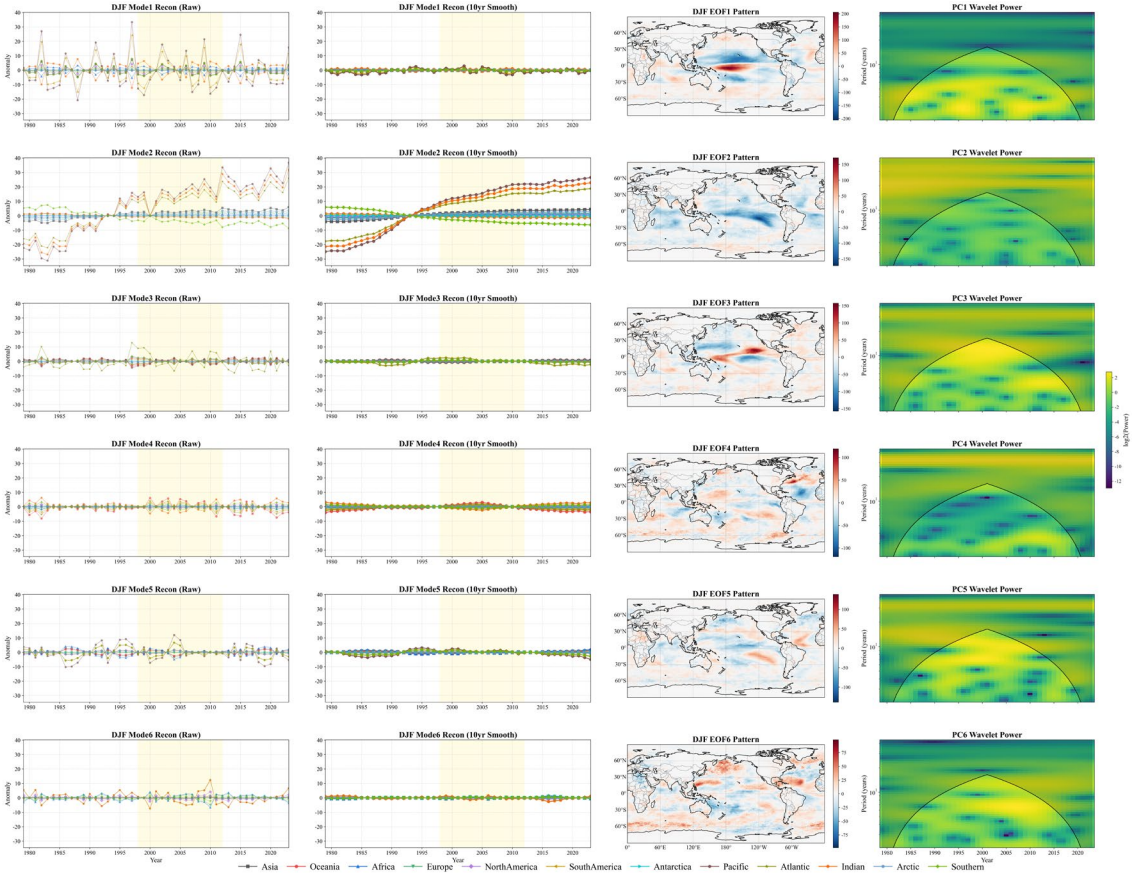

Figure S5 Same as Figure S1, but for winter.